Intermittent behavior in slow drainage

Liv Furuberg, Knut Jørgen Måløy, and Jens Feder
Department of Physics, University of Oslo, Box 1048, Blindern, 0316 Oslo, Norway
(Received 16 March 1995)

The water pressure measured during slow, constant rate drainage in a two-dimensional porous model exhibits sudden jumps as bursts of air quickly displace water from a region. The measured size distribution of the pressure jumps is exponential. Invasion percolation (IP) simulations give a power-law size distribution of the connected regions invaded in bursts. In the experiments the meniscii of the fluid-fluid front adjust during a burst, causing the capillary pressure to decrease. Including this effect in a modified invasion percolation algorithm causes potentially large bursts to split up into smaller bursts that are exponentially distributed. From the experimental pressure curve it is possible to identify groups of bursts that would become a single, "composite" burst in a larger system. These composite bursts are power-law distributed, consistent with simulations and percolation theory. Different versions of the IP model result in different structures and power-law exponents. The best choice of model for the present experiment is discussed.

PACS number(s): 47.55.Mh, 05.40.+j, 47.55.Kf

I. INTRODUCTION

The displacement of one fluid by another in porous media has been the object of intense studies because such processes are able to create a rich variety of front structures depending on the relative viscosities, the wettability, and the displacement rate. Drainage processes in porous media are of interest both from a practical and theoretical point of view. In the limit of very slow displacement, the structure of the invading fluid has been shown [1] to be fractal [2,3], and the process has been modeled by the invasion percolation (IP) algorithm [4–6].

This paper presents measurements on a two-dimensional porous model system where air displaces water at a constant *rate*, resulting in a fluctuating pressure difference between the fluid phases [7]. Corresponding modified IP simulations display similar pressure fluctuations. It is observed experimentally that with the constant pumping rate, the front movement is not continuous. In periods when the pressure difference across the air-water front builds up, the interface between the fluids is stable. Air invasion of a smaller or larger area of the porous medium in a sudden burst accompanies an abrupt decrease in the pressure difference. The appropriate IP model for simulation of the present experiment is discussed, and a modified IP model is introduced and explored.

Haines [8] and later Morrow [9] described qualitatively this type of invasion behavior in bursts for drying processes where evaporation of water from a heap of glass spheres (or agricultural soils) caused all the air-water meniscii to continuously withdraw slightly inside the pore throats for some time. Between these stable periods bursts occurred where larger or smaller regions of the medium were dried out. The pressure in the water decreased slowly in the stable periods but exhibited a sudden increase every time a region was invaded by air. Such jumps have been termed Haines jumps. The dynamics of drying can be described by the algorithm presented here, with the modification that the evaporation rate is not constant, but slows down as the distance between the fluid-air front and the open edge of the system increases. The geometric structure of drying fronts was previously modeled by an IP algorithm [10,11]. Thompson *et al.* [12] studied a related system, measuring jumps in electrical resistance in mercury invasion experiments in three-dimensional porous media. They observed a power-law distribution of the resistance jumps consistent with simulations [13]. This is, however, not comparable to our measurements since not all invasion is reflected in the resistance.

Recently, much interest has been focused on driven systems exhibiting dynamic behavior with stable periods, where energy is slowly fed into the system, interrupted by sudden events when smaller or larger amounts of energy are dissipated. Intermittent behavior with power-law distribution of relaxation events is characteristic of "self-organized criticality," a type of behavior in which driven systems automatically evolve towards a critical state [14]. Examples of systems with intermittent behavior count different types of spring-block systems with stick-slip motion [15–17]. Simple experimental spring-block systems [15,17] exhibit dynamic behavior very similar to that of our drainage experiment. There is, however, a difference between these systems and IP: In self-organized critical systems, disorder is produced dynamically from the initial conditions and/or the randomness in, for example, dropping grains. IP models have quenched disorder that is given by the random medium when the experiment starts. In addition, the IP model is *critical* only in zero-gravity field.

In this paper we present an analysis of the water pressure measured during displacement of water by air. The

distribution of pressure jump heights is found to be exponential. We demonstrate that the experiments are modeled by a modified IP algorithm that takes into account the incompressibility of water, which causes the capillary pressure to decrease abruptly during a quick displacement in a burst. With this effect included in the algorithm, we obtain a realistic time evolution of the water pressure. On the other hand, the parameters may be varied in the simulations, the meniscii can be assigned a large ability to adjust, or the front can be defined to be long. In this case we obtain a power-law pressure jump distribution. It is in principle possible, but it will be difficult to construct a large experiment where power-law distributions of pressure jumps can be measured over any significant range of sizes. For systems comparable to the experiments with small system sizes and fronts that can only adjust slightly before one meniscus breaks, simulations show that the large bursts break up and an exponential distribution of jumps is obtained in accordance with the experiments.

The geometric sizes of regions invaded in bursts are roughly proportional to the accompanying pressure jumps. The exponents governing the power-law distribution of geometric burst sizes in slow drainage was related to percolation [18] exponents independently by two groups: Martys *et al.* [19] used finite-size scaling techniques, and Gouyet and co-workers [20,21] initially studied diffusion front fluctuations and argued via the probability of connection and disconnection of finite percolation clusters to the front. Our simulation results confirm their scaling predictions for burst-size distributions for all three possible cases of IP simulations in two dimensions: The front where the IP cluster is allowed to grow is defined as (1) the Grossman-Aharony external perimeter [22], (2) the hull [23], or (3) the full perimeter; the union of the outer hull and inner hulls surrounding finite defender regions.

It is demonstrated that the simulated pressure curves can be analyzed in a way that permits us to extract the underlying power-law distributions also from pressure curves that have an exponential jump size distribution. The power law extracted from the experimental curve by this method is consistent with the IP model results and is thus described by percolation exponents. This is therefore an example of a real system with intermittent behavior that can be mapped to a familiar model, the IP model.

The paper is structured as follows. In Sec. II we review the physical mechanisms that govern the slow drainage in porous media, while Sec. III presents the experiment and the experimental results. The modified IP algorithm is defined in Sec. IV, where also the validity of the model is discussed. Simulation results such as burst-size distribution and cutoff, waiting time distribution, and results of interest for the theory of IP are presented in Sec. V. In Sec. VI simulation parameters are estimated from the experiments and the burst-size distribution obtained in simulations is compared both to the experimental burst-size distributions and the "composite bursts" obtained from experimental pressure curves. A summary follows in Sec. VII.

II. MECHANISMS OF SLOW DRAINAGE IN POROUS MEDIA

The process where a nonwetting fluid (air) displaces a wetting fluid (water) from a porous medium is called drainage. As discussed in the Introduction, IP patterns are generated during slow drainage. Changes in the invaded pattern with the wetting properties of the fluids were studied by Martys *et al.* [24]. When the invading fluid becomes more wetting, the growth becomes correlated and self-affine fronts appear [25]. Our experiment is in the regime where the displaced fluid wets the medium well, front segments move independently, and self-similar structures are created. The characteristic of a *slow* displacement process is that viscous pressure gradients have time to relax between front movements and capillary effects govern the displacement.

The porous medium has open interconnected pores of fluctuating size, with a mean pore size a. We describe displacement that is caused by water being pumped out of the system at a slow, constant rate causing air to be pulled in from an open edge at the same rate. The dynamics is identical to that of displacement due to air being injected into the model at a constant rate. At some stable stage of the displacement process, the air has invaded a region of the void space, and the air-water interface is broken up into meniscii that meet the solid grains of the medium with a contact angle determined by the wetting properties of the fluids (see Fig. 1). The pressure difference p_{cap} between air and water (the *capillary pressure*) is the same everywhere along the front and $p_{\mathrm{cap}} = \gamma(1/r_1 + 1/r_2)$ where γ is the interfacial tension and r_1 and r_2 are the principal radii of curvature of the interface. When water is pumped out of the system, the meniscii are pulled slightly towards more narrow parts of the pores and the local radii of curvature decrease causing an increase in the capillary pressure. If the capillary pressure between the fluids becomes larger than the *capillary pressure threshold* (the equilibrium capillary pressure of the narrowest part of the pore) of the broadest pore neck, the front becomes unstable at this position. The air-water meniscii proceed quickly to find a new stable position. Many pores can be invaded by air in such a *burst* if pores with low capillary pressure thresholds are encountered after the breakthrough in one pore throat. The size of a burst is defined as the number of pores s that are invaded from the instant the interface becomes

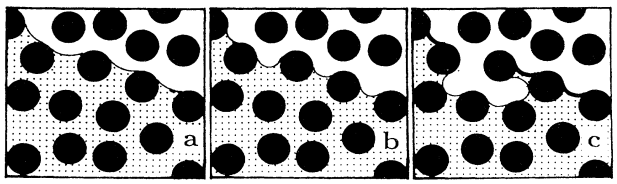

FIG. 1. (a)–(c) Invasion of air (white) into a two-dimensional porous medium initially filled with water. As water is extracted, the interface moves into narrower parts of the pore necks. During a burst, new pores are invaded and the interface adjusts everywhere back to the lower capillary pressure.

unstable until it finds a new stable configuration. Since the pumping rate is very slow compared with the time scale of a burst, the water volume that is displaced when air invades the new pores must be pushed towards the adjustable front meniscii, causing the meniscii to quickly readjust back to larger radii and the capillary pressure to decrease in a jump. The ability of the interfacial meniscii to receive or give up a capacitive volume of water due to small readjustments of the meniscii is thus responsible for the Haines jumps.

Starting a burst from a quite high value of the capillary pressure, it decreases at some rate down to a capillary pressure that is too low for further invasion. The total amount of water that the front is in position to receive after one meniscus breaks, before the pressure becomes too low for continuing invasion, puts an upper limit on the size of the burst. The rate of change in the average volume of water received in a front pore with the capillary pressure is defined as the *volume capacitance*

$$\kappa = dv/dp_{\mathrm{cap}}, \tag{1}$$

$[\kappa] = m^5/N$, where v is the average volume of water received in an interfacial pore since the beginning of the burst. We assume κ is a constant. This is a simplification because the water volume received by the front is not necessarily linearly dependent on the capillary pressure, or constant over the pressure range, and hysteresis effects will occur when the meniscii move back and forth. The maximum available volume V_f that the front is in a position to receive when a meniscus breaks and a burst starts is then given by the product of the number n_f of pores at the interface, the volume capacitance, and the average capillary pressure threshold p_{start} where a burst starts: $V_f \propto \kappa p_{\mathrm{start}} n_f$. The magnitude of the capillary pressure jump Π accompanying a burst is proportional to the size s of the region spontaneously invaded and inversely proportional to κn_f: $\Pi \propto s/(\kappa n_f)$. As noted by Morrow [9], pressure jumps of visible size are a characteristic of small systems only. An argument for this statement is found in Sec. V, Eq. (7), where we show that the typical largest burst size grows more slowly with the system size than does the front length n_f.

A burst has a characteristic time scale τ_{cap} that depends on the viscosity of the fluids, a typical capillary pressure jump, and the size of the system. If the pumping rate is so large compared to the time scale of a burst that a significant amount of water is pumped out of the system during a burst, the structure of the invaded area will be changed due to viscous pressure gradients, and the IP algorithm is no longer a good model for the displacement. Furthermore, the burst-size distribution will be changed, and the burst sizes will not be limited by the water volume that can be received by the front.

The time scale of a burst can be roughly estimated by the following argument: The meniscus that is situated at the typically largest possible distance L (the system size) from the burst region will relax most slowly, because the flow of water from the burst area to the meniscus will be driven by a pressure gradient of the order p_{cap}/L. The water velocity close to the meniscus is then approximated by Darcy's law: $U \sim -(a^2 p_{\mathrm{cap}})/(\mu L)$ where μ is the viscosity of water, a is the mean pore diameter, and a^2 is a rough estimate of the permeability. This must equal the meniscus velocity given by the capillary pressure-volume relation [Eq. (1)]: $U \sim d(\kappa p_{\mathrm{cap}}/a^2)/dt$, where a^2 is a characteristic cross section of a pore. By setting these velocities equal to each other we obtain an exponential relaxation of the capillary pressure at the remote meniscus position with a characteristic relaxation time $\tau_{\mathrm{cap}} = (\mu L \kappa)/a^4$. By dimensional analysis $\kappa = a^4/\gamma$, so that $\tau_{\mathrm{cap}} = \mu L/\gamma$. This time scale must then be compared with the time scale τ_p for the pumping rate: $\tau_p = a/v_q$ where the fluid velocity v_q in a typical pore is given by the pumping rate q divided by the number of pores L along the edge where water is withdrawn: $q = v_q L$. The ratio of these characteristic times gives a "capillary number"

$$\mathrm{Ca}^* = \frac{\mu v_q}{\gamma}\frac{L}{a}. \tag{2}$$

Note that this capillary number depends on the size of the system. We expect a crossover to viscous fingering when the length scale L is increased and the pumping rate per pore along the outlet is kept constant.

III. EXPERIMENTS

The two-dimensional model was constructed by a monolayer of 1 mm glass spheres between two 25 mm Plexiglas plates (see Fig. 2). The model is transparent and has a porosity of $\phi \simeq 0.7$ and an average pore volume $\Omega \simeq 2$ mm^3. To provide the boundaries of the model we used a rectangular silicon rubber packing. Since the edges of the packing are straight we also applied silicon glue to prevent increased permeability at the boundaries. An air pillow was inserted between the lower Plexiglas plate and the glass beads to keep the beads in contact with the upper plate. During the experiment, water was withdrawn from one short side of the model with a syringe pump at a low *constant rate* of $q = 0.048$ pore/s, and the other side was open to atmospheric pressure for invasion of air.

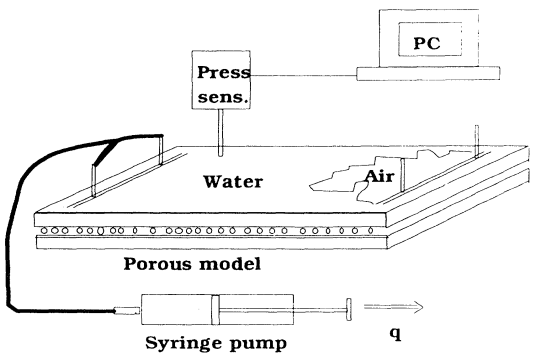

FIG. 2. Experimental setup. Quasi-two-dimensional porous medium with pressure sensor in the water phase. Water is pulled out at one edge by a syringe pump, while air invades from the opposite edge that is open.

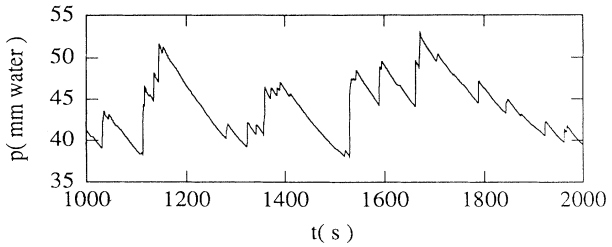

FIG. 3. Water pressure as function of time during drainage. The water pressure decreases steadily in stable periods as water is slowly extracted from the system. Air invasion takes place in bursts accompanied by sudden positive jumps in the water pressure.

The ratio of the characteristic time scales of the relaxation of the front in a burst and that of pumping is in this case $Ca^* = 1.3 \times 10^{-6}$ [Eq. (2)]. Thus the front will relax between bursts and the pumping rate does not affect the single burst developments.

Pressure fluctuations were measured with a pressure sensor of our own construction [26] connected to a personal computer (PC). The sensor uses an electronic balance as the main component and is linear over four decades with a resolution of 0.1 mm H_2O and a time response of about 1 s. The water pressure is measured at one single point in the water phase. This point is not very close to the water-air interface. During a burst, local pressure fluctuations due to quick meniscus movements occur close to the fluid-fluid interface. These fluctuations are not registered by the pressure sensor. The pressure measurements are reliable only in the buildup phase, including the pressures where a burst starts and stops. There is no information about the capillary pressure during a burst, as indicated by the almost vertical pressure jumps that occur for each burst, see Fig. 3.

An experiment consisted of about 70 000 pressure measurements taken at 1 s intervals (see Fig. 3). The bursts were identified as sharp positive pressure jumps that were larger than 0.1 mm H_2O.

IV. MODIFIED INVASION PERCOLATION

The algorithm is a modified version of ordinary invasion percolation [4], where the path of least resistance is found through a disordered medium. In the modified algorithm presented here, the geometry of the invaded structure is identical to that of IP, but the dynamics is different.

A. Algorithm

A square lattice of size $L_1 \times L_2$ that consists of nodes (pores) connected by bonds (throats) represents the porous medium. Bonds are assigned random numbers p_i drawn from a uniform distribution in the interval [0,1], representing capillary pressure thresholds in the throats. Nodes are defined to have a unit *volume*. Initially the lattice is filled by "water" (the defender). "Air" (the invader) is injected from the source, which is defined to be one of the short sides of the lattice, at a *constant rate* of one unit volume per time unit. The defender escapes at the sink at the opposite side at the same rate. Nodes inside the lattice are, however, not invaded at a constant rate, modeling that the injected volume can both be stored along the fluid-fluid front (this air volume is invisible in the simulated invaded structure) or invade full nodes.

The initial capillary pressure is $p_{\rm cap}(0) = 0$. During the invasion $p_{\rm cap}$ develops dynamically as described below, and is confined between 0 and a value slightly above $p_c = 0.5$. A bond can be invaded only if it belongs to the growth zone, meaning that it neighbors either the source or the present invaded cluster, and if $p_{\rm cap}$ is equal to or larger than the capillary pressure threshold p_i in that bond. If more than one available bond have $p_i < p_{\rm cap}$, the bond with the smallest p_i is chosen first for invasion. The capillary pressure of the model at time t is simply defined to be proportional to the difference between the *total* injected air volume $V = t$ (which is the sum of the air volume that is stored by the adjusted meniscii along the front and the air volume in invaded pores), and the volume N of all sites (pores) that are invaded by air at this stage. The difference $V - N$ then corresponds to the excess air volume stored along the front (physically by adjusting the meniscii):

$$p_{\rm cap}(t) = (V - N)/(n_f \kappa). \tag{3}$$

The capillary pressure is inversely proportional to the front length n_f, the number of bonds connecting invaded sites to uninvaded sites. The linear relation between the average excess air volume $v = (V-N)/n_f$ per throat and the capillary pressure $p_{\rm cap}$ is then defined by the volume capacitance κ [see Eq. (1)]: $\kappa = v/p_{\rm cap}$.

The following algorithm was used in the simulations.

(1) Initially the growth zone consists of the L_1 sites that neighbor the source ($n_f = L_1$), and the pressure difference is $p_{\rm cap}(0) = 0$.

(2) The site in the growth zone that has the bond with the smallest $p_i = p_{\rm min}$ is identified.

(3) The capillary pressure $p_{\rm cap}$ increases linearly with time until $p_{\rm min}$ is reached at time t_1, where $t_1 = p_{\rm min} n_f \kappa$.

(4) The bond containing $p_{\rm min}$ and the connected site (one volume unit) is invaded and the capillary pressure decreases from $p_{\rm min}$ to $p_{\rm cap} = p_{\rm min} - 1/(n_f \kappa)$.

(5) The growth zone is modified due to the invaded site.

(6) The site in the new growth zone that has the bond with the smallest $p_i = p_{\rm min}$ is identified. If p_i is smaller than $p_{\rm cap}$, this site is invaded, and the capillary pressure is decreased further. Continue to find the easiest invaded site until $p_{\rm min} > p_{\rm cap}$. At this stage s sites have been invaded in a burst and the total capillary pressure jump is $\Pi = -\sum_1^s 1/(n_f \kappa) \simeq -s/(n_f \kappa)$.

(7) The capillary pressure $p_{\rm cap}$ is increased linearly with time until $p_{\rm min}$ is reached at time $t_2 = t_1 + (p_{\rm min} - p_{\rm cap}) n_f \kappa$.

(8) Repeat from (3).

At step (5) the new growth zone is identified after in-

vasion of one site. If the newly invaded site has closed off some region of the defender so that this region is not connected by defender sites to the sink, all growth zone sites in this region are removed from the growth zone. This is called a trapping rule, and it accounts for the incompressibility of the defender.

Moreover, in this modified IP algorithm, a trapping rule is essential for the system to reach a stationary state with an average front length, and thus an average capacity to take up excess air. Without a trapping rule the growth zone would surround defender islands that are left behind the front, and the average front length would continue to increase throughout the simulation.

Only two different types of growth zones are possible for IP with trapping, because all *outer* perimeters of percolation clusters in two dimensions fall into two classes depending on the connectivity rules of the two phases: The Grossman-Aharony perimeter, called the *external perimeter* [22], and the *hull* [23]. On a square lattice, allowing sites to be connected through nearest neighbors only in both the invaded and the defender phase, the growth zone is the external perimeter. The length of the growth zone then scales with the system size L_1 as $n_f \propto L_1^{D_e}$, where $D_e = 1.34$ [22]. Letting the defender phase connect both via nearest neighbors and next nearest neighbors gives a hull growth zone with a length $n_f \propto L_1^{D_h}$, where $D_h = 1.75$ [23]. We have simulated IP with both types of growth zones, and in the following D_f will denote the fractal dimension of the front in expressions valid for both perimeters.

Many of the simulation results presented in this paper are obtained from simulations with randomness in bonds, as described above, and external perimeter growth zone. In addition we performed simulations with randomness in the sites instead of the bonds, always invading the available site containing the smallest random number. In this case simulations with both external perimeter and hull growth zone were carried out. The influence of bond or site randomness on the growth zone dimension has been investigated by Meakin [27]. In agreement with Meakin we observe that the effective fractal dimension of the external perimeter for the present system sizes changes from $D_e = 1.30 \pm 0.03$ for randomness in bonds to $D_e = 1.39 \pm 0.02$ [28] for randomness in sites.

B. Validity of model

The IP rule of choosing the easiest throats models a system where there are no viscous pressure gradients in the fluids. It has been supposed that this is fulfilled in the limit of very slow displacement. The experimental pressure curves show, however, that even if the displacement rates are small, the actual displacements take place quite quickly during bursts. We argue that even if there are viscous pressure gradients locally in the fluids during a burst, the total structure of the displaced area in a burst may remain quite unaffected: Consider a burst starting at the capillary pressure p_{cap}. During the quick displacement, the capillary pressure can never be larger than p_{cap}. This confines the area available to burst invasion to that of IP, even if the order of pore invasion is not exactly the same as in IP.

In the simulation model, the capillary pressure is defined during a burst as decreasing by $\delta p = 1/(n_f \kappa)$ after invasion of one site with a unit volume. This does not necessarily correspond to the physical pressure during a burst, but it gives a good approximation of the correct pressures at the points where a burst starts and stops. The area invaded in a burst in the simulations is believed to be roughly correct even if in the experiments the local displacement may take place in a different order than always choosing the broadest available throat due to viscous pressure gradients.

It is clear that there would be physical bounds on κ if we were simulating drainage in a real porous media formed like a lattice with varying throat widths. The volume stored per pore throat along the front by adjusting meniscii will in such porous media that are realizable not be larger than the order of one pore volume. This must be an upper bound on the volume stored in an average pore throat when the meniscus breaks at a p_{cap} which in the simulations is limited from above by p_c where $p_c = 0.5$. With an average volume $v_{\max} = 1$ stored per pore throat when a meniscus breaks, the maximal κ will be of the order $\kappa = v_{\max}/p_c = 2$. In the next section we will freely use any value of κ for theoretical considerations. The combined parameter κn_f decides the capacitive volume and therefore the largest obtainable burst. Simulations with a large value of κ combined with a realizable system size will therefore indicate how even larger physical systems with smaller and physical values of κ would behave.

V. SIMULATION RESULTS

Invasion percolation structures are known to be fractal [2,3]. The number of sites s in a cluster scales with the linear cluster size ℓ as $s \propto \ell^D$. For IP without trapping $D = 1.89$ [18], while for IP with a growth zone restricted to the hull or the external perimeter of the invaded structure the fractal dimension has been measured to be roughly in the range $1.86-1.89$ [29] and 1.83 [4,27], respectively. The effect of the modified IP algorithm with a limited volume capacity is to split the invaded structures into smaller bursts. In an ideal system of infinite size and infinite capacitive volume in the front and no trapping, the bursts would roughly be percolation clusters at p_c. The burst-size distribution, however, differs from the cluster size distribution of percolation because the invading structure does not include all clusters but it only reaches the subset of all percolation clusters that is situated close to its perimeter.

A. Burst-size distribution

A burst is *ideally* defined as the connected structure of sites that is invaded following one root site that grows from the perimeter of the existing invaded region [29]. All sites in the burst have random numbers smaller than the root site and the burst will not touch the old invaded

region at any other sites than the root. The introduction of the capacitive volume implies that not all available sites with random numbers smaller than the root will be invaded in one burst, the capillary pressure decreases during the burst and may have to be increased before further invasion in a new burst can take place. If the capacitive volume is infinitely large, we obtain the ideal case where bursts are not split up. The typical largest burst sizes in the distributions depend on the front length of the invaded structures L^{D_f}, the volume capacitance κ, and the capillary pressure at which meniscii break and bursts start. The burst-size distribution $N(s)$ for different values of κL^{D_f} can be written on a scaling form:

$$N(s) \propto s^{-\tau'} f(s/s^*), \tag{4}$$

where s^* is the typical largest burst size, depending on κL^{D_f} as explained below. When $s \ll s^*$, the crossover function f is a constant, while it is exponentially decreasing when $s \gg s^*$. A relation between τ' and percolation exponents was found independently in Ref. [19] (for external perimeter growth zone) and in Ref. [21] (for hull growth zone). They suggest that the burst-size distribution exponent equals

$$\tau' = 1 + D_f/D - 1/(D\nu). \tag{5}$$

This relation gives $\tau' = 1.53$ for the hull perimeter (with D_h chosen to be 1.86) and $\tau' = 1.32$ for the external perimeter (randomness in bonds) when the front and structure fractal dimensions are substituted for each case. The percolation correlation length scaling exponent is $\nu = 4/3$. In Fig. 4 simulation results from IP with a hull growth zone and randomness in sites are shown. The exponent τ' is estimated to be $\tau' = 1.48 \pm 0.05$. Similar simulations for IP with external perimeter growth zone and randomness in bonds give $\tau' = 1.30 \pm 0.05$ [7]. We thus confirm Eq. (5) for IP in both cases of external perimeter growth zone and hull growth zone [30].

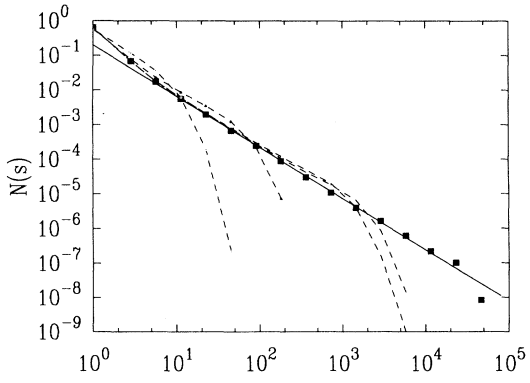

FIG. 4. Simulated burst-size distribution for different parameter values of (L, κ): (200, 0.01) falling off most quickly, (300, 0.1), (200, 10), (300, 10), and (300, 1000) having the longest power-law regime. The last data (L, κ)=(300, 1000) are shown as solid squares. IP with randomness in sites and hull growth zone, curves averaged over 200 samples. The straight line shows the best estimate of the exponent $\tau' = 1.48$.

The sizes of the pressure jumps are on average proportional to the geometrical size s of the burst $\Pi \propto s/(\kappa L^{D_f})$. Transformation of variables in the distribution function Eq. (4) gives the power-law behavior $n(\Pi) = \Pi^{-\tau'} f(\Pi/\Pi^*)(\kappa L^{D_f})^{1-\tau'}$ for the size distribution of pressure jumps.

B. Cutoff on the burst-size distribution

In Fig. 4 the power-law burst-size distributions are cut off by a characteristic largest cluster size s^*, which depends on the values of L and κ through the characteristic available volume stored in the front when a burst starts. This volume will limit the largest size of the burst. The following argument gives the characteristic burst size s^* for a chosen value of κL^{D_f}. Consider a burst starting at the critical pressure p_c. After the first site is invaded, the pressure has decreased to $[p_c - 1/(\kappa n_f)]$. In percolation, the correlation length ξ scales with the distance to p_c: $\xi \propto (p_c - p)^{-\nu}$, where ν equals 4/3 in two-dimensional (2D) percolation. When the size of the burst is $s = 1$, the correlation length restricting the burst size is $\xi \propto (\kappa n_f)^{\nu}$. The characteristic largest burst size is reached after invasion of s^* sites, when the correlation length is of the order of the linear size of the cluster:

$$\xi \propto (p_c - p^*)^{-\nu} \propto \left(\frac{s^*}{\kappa n_f}\right)^{-\nu} \propto \left(\frac{s^*}{\kappa L^{D_f}}\right)^{-\nu} \propto (s^*)^{1/D}. \tag{6}$$

The typical largest cluster size hence scales as

$$s^* \propto (\kappa n_f)^{\nu D/(1+\nu D)} \propto (\kappa L^{D_f})^{\nu D/(1+\nu D)}. \tag{7}$$

This scaling behavior is documented in Ref. [7]. The characteristic pressure p^* scales as $(p_c - p^*) \propto (\kappa L^{D_f})^{-1/(1+\nu D)}$ from Eq. (6), indicating that introducing a finite volume capacitance has the effect of removing the dynamics of the system from criticality at p_c, while the geometric structure is unaffected. The capacitive volume effect results in that bursts are broken up and most bursts start at values lower than p_c around p^*. Figure 5 shows the simulated pressure curve for a system where $p^* = 0.37$. The capillary pressure curve is turned upside down relative to the water pressure curve in Fig. 3, because the capillary pressure increases when the pressure in the water decreases. The characteristic pressure p^* is calculated from $(p_c - p^*) = A(\kappa L^{D_e})^{-0.28} = 0.13$ (the constant $A = 0.44$ was measured from Fig. 7, see below). It is observed from Fig. 5 that the bursts indeed start at pressures spread around $p^* = 0.37$. The value D_e is used in the calculation because the simulations use the external perimeter growth zone.

The distributions of pressures where the bursts start, p_{start}, are shown in Fig. 6 for different values of κL^{D_f}. It is seen that for large values of κL^{D_f} all bursts start close to p_c, resulting in a large power-law regime of the burst-size distribution. In the other limit of very small κL^{D_f}

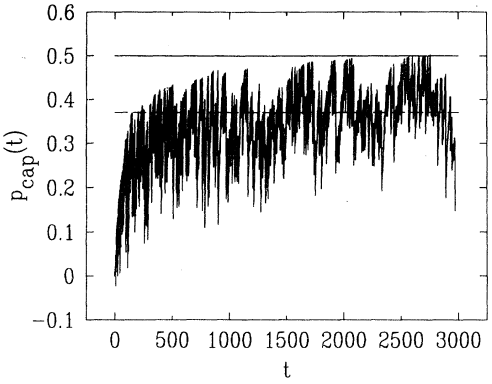

FIG. 5. Simulated capillary pressure curve for a system of size $L = 100$ and volume capacitance $\kappa = 0.2$ with a total of 2800 invaded sites. Upper horizontal line is at $p_c = 0.5$, lower dashed line at $p^* = 0.37$, the characteristic pressure for this process.

every burst would contain one site only, and the distribution of p_{start} would be roughly uniform between zero and p_c. The rescaled distributions (see Fig. 7) show that the most probable $p_{\text{start}}(\kappa L^{D_e})$ is at $p_c - p^* = 0.44(\kappa L^{D_e})^{0.28}$ and there is a good data collapse for different values of κL^{D_e}. The small deviations for rescaled pressures smaller than zero come from the finite system sizes. The rescaled pressures in this range correspond to sites with p_{start} larger than p_c that have to be invaded in order to penetrate the lattice. The number of these sites depends solely on the lattice size, and invasion in smaller systems will be forced to invade more values higher above p_c. Finite-size effects due to the deviation from p_c given by the lattice size itself, $(p_c - p) \propto \xi^{-1/\nu} \propto L^{-1/\nu}$, will govern the cutoff burst size if this correlation length is smaller than that given by the finite capacity effect. The capacity of the front decides the maximum burst size if $L > (\kappa L^{D_f})^{\nu/(1+\nu D)}$, or equally $\kappa < L^{1/\nu+D-D_f}$. This is fulfilled for the rescaled results shown in Fig. 7.

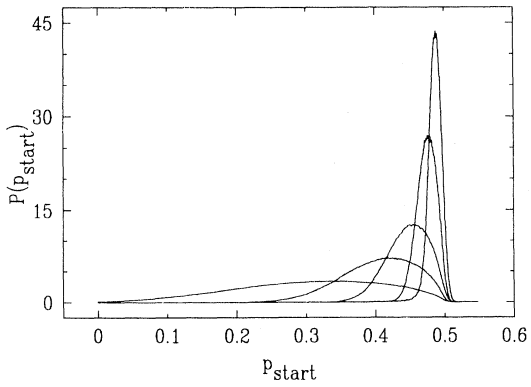

FIG. 6. Simulated distributions of pressures p_{start} where bursts start for different combinations of the system size L_1 and the capacity κ (L, κ). Broadest distribution: $(300, 0.01)$, then $(400, 0.1)$, $(300, 1)$, $(400, 10)$, and $(300, 100)$ for the narrowest distribution. All curves are averaged over 200 simulations. The simulations have randomness in bonds and external perimeter growth zone.

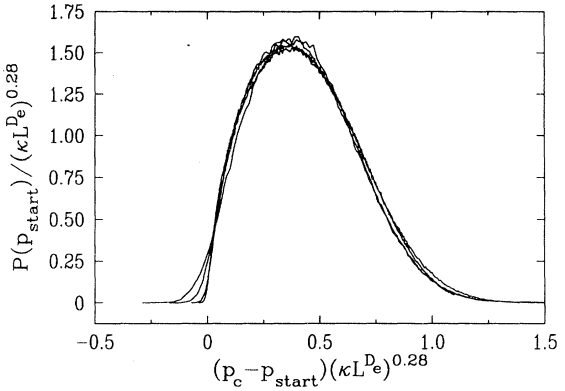

FIG. 7. Rescaled and collapsing distributions of pressures where bursts start, same combinations of parameters as in Fig. 6.

C. Waiting time distribution

The simulations start with a zero pressure difference between the phases. Initially, the injected volume will mainly result in a larger excess "air" volume stored along the front, and a higher capillary pressure. After the pressure reaches $p_c - p^*$ for the first time, it will continue to fluctuate around this value, and the volume that is injected into the model in a time period is on average equal to the number of sites (with unit volume) invaded in the same time period. We measured the waiting times Δ between successive bursts in the stationary invasion regime $\Delta = t_n - t_{n-1}$, where t_n denotes the time when burst number n occurred. The waiting time distribution for different values of κL^{D_f} is shown in Fig. 8. The distributions are exponential for small κL^{D_f}, consistent with experiments [7]. For larger capacitive volumes, the distributions are more difficult to characterize. They are, however, *not* power-law distributed.

The average waiting time between two successive bursts, averaged over M bursts in the stationary inva-

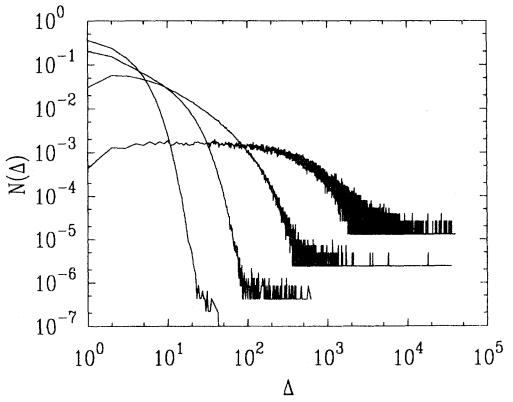

FIG. 8. Simulated distributions of waiting times between two subsequent bursts for different values of (L, κ): (300, 1000) lowest curve, (200, 10), (300, 0.1), (200, 0.01) upper curve. IP with randomness in sites and with hull growth zone, curves averaged over 200 samples.

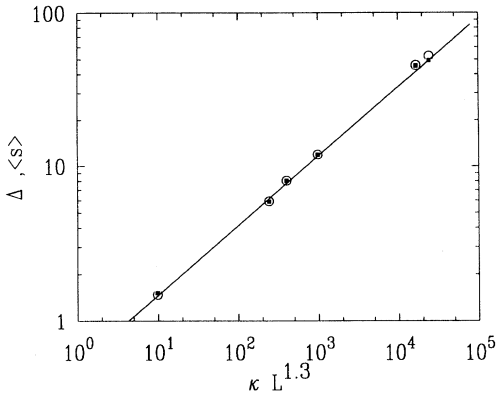

FIG. 9. Average waiting time between subsequent bursts (open circles) and average burst sizes (small solid squares) as a function of κL^{D_e}. Each point is averaged over 200 samples. Straight line has slope 0.45. The simulations have randomness in bonds and external perimeter growth zone.

sion regime, is defined as $\langle\Delta\rangle = (1/M)\Sigma_{n=1}^{M}(t_n - t_{n-1})$. The average waiting time diverges when $\kappa L^{D_f} \to \infty$ as $\langle\Delta\rangle \sim (\kappa L^{D_f})^{\gamma'}$. The average burst size $\langle s\rangle$ is expected to diverge with the same exponent, because the average burst size must equal the average air volume pumped in between bursts in the stationary regime. The relation between the scaling exponent γ' and percolation exponents is found by calculating the first moment of the burst-size distribution [Eq. (4)] as a function of $\kappa L^{D_f} = (p_c - p^*)^{-(1+D\nu)}$, expecting the average burst size to increase when $(p_c - p^*) \to 0$. We obtain $\langle s\rangle \sim \int sN(s)ds \sim (\kappa L^{D_f})^{(1+D\nu-D_f\nu)/(1+D\nu)}$, where $\gamma' = (1 + D\nu - D_f\nu)/(1 + D\nu) = 0.46$ when $D = 1.83$ and $D_f = 1.39$. The average waiting time between successive bursts is measured for the case of site IP with external perimeter growth zone, and the average waiting time is found to scale in good accordance with theory as (see Fig. 9) $\langle\Delta\rangle \sim (\kappa L^{D_e})^{\gamma'}$, with $\gamma' = 0.46 \pm 0.02$.

Figure 10 shows that the average waiting time $\langle\Delta(s)\rangle$ immediately before a burst of size s is always independent of the size of the burst. This means that on average the system is not stable for any longer time period immediately before a huge burst than it is preceding a small burst. The large fluctuations in $\langle\Delta(s)\rangle$ for large burst sizes are due to poor statistics.

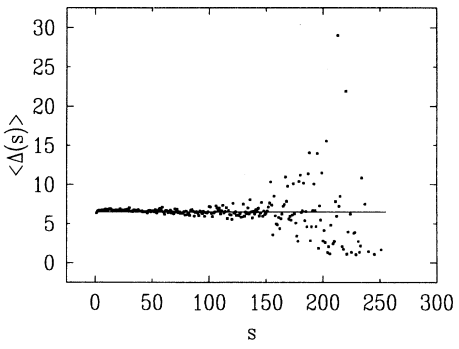

FIG. 10. Mean waiting time immediately before a burst of size s. Averaged over 200 samples.

D. Sequence of random numbers

In the simulations we can obtain information that is not available from the experiments: the precise value of the random numbers, representing the capillary pressure thresholds, in the sites that are invaded. This section presents results from analysis of this sequence that confirm a recently published theory on scaling in growth models [31]. The sequence of random numbers in the successively invaded sites $p_{\min}(N)$, where N is the number of invaded sites, was first analyzed by Roux and Guyon [29] (Fig. 11). This curve contains much more information than the pressure curve obtainable in experiments, because the experimental pressure curves only give a knowledge of the capillary pressure thresholds in the pore throats where bursts start. The rest of the capillary pressure thresholds are hidden in the pressure jumps.

Roux and Guyon [29] suggested that in IP simulations (corresponding to an infinite κL^{D_e} in our case) the burst sizes could be extracted from the sequence of random numbers. Starting from one invaded site containing the random number $p_{\min}$, count the number of sites successively invaded after this site that are connected to the previous invaded structure by this site only. This is the case for all following sites with random numbers smaller than $p_{\min}$. The number of sites invaded in a connected cluster will then be defined as a *valley* in the sequence of random numbers. We found the distribution of all valleys starting in a narrow strip immediately below p_c for simulations with both external perimeter and hull growth zone. In both cases we found power-law distributions of valleys, governed by exponents described by Eq. (5), and with a cutoff due to the system size only. The difference between valleys and bursts is that valleys can be defined to start at values confined to a narrow strip, while bursts start at capillary pressures determined by the system and distributed as shown in Fig. 6.

In Sec. IV we concluded that IP without trapping would result in an ever growing perimeter of the invaded structure, and no stationary regime for the capacitive air volume would be reached. We are, however, free to find

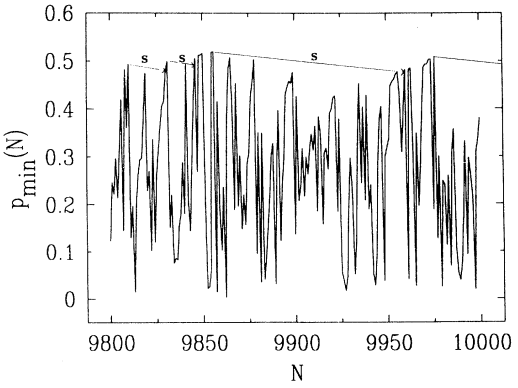

FIG. 11. Sequence of invaded random numbers $p_{\min}(N)$ (capillary pressure thresholds). Lines with slope $1/(n_f\kappa)$ start at some invaded random numbers where bursts start. The burst size is the number of invaded sites before the line hits the curve.

the valley size distribution of the sequence of random numbers also in the case of no trapping. The valley size distribution will correspond to the burst distribution in an unphysical, ideal system with an infinite volume capacity that does not depend on the front length. In this way we will be able to check Eq. (5) for IP without trapping. The cumulative valley distribution of valleys starting at random numbers between 0.580 and 0.595 is shown in Fig. 12, for site IP. Note that valleys are allowed to proceed in parallel, but this will not happen frequently since the strip is narrow. The power-law exponent was measured to be $\tau' = 1.60 \pm 0.02$. This value satisfies Eq. (5) with $D_f = D$. The size distribution of percolation clusters split off by removing one bond is governed by the same exponent [32,33].

Hierarchical forward bursts are defined to start at every invaded site (every random number in the sequence) and to proceed forwards until the horizontal line hits the sequence of random numbers curve again. The distribution of forward hierarchical bursts is shown as the lower curve in Fig. 12. The hierarchical burst-size distribution is found to decrease as a power law with an exponent $\tau_f^{\text{all}} = 2.00 \pm 0.01$ for all three trapping rules in two dimensions. Maslov [31] recently showed that this result is true for a class of invasion models including also the interface depinning model [34] and the Bak-Sneppen evolution model [35]. Hierarchical bursts start in the range 0–p_c while bursts start in a narrow range of p values. Maslov argued that the invaded random numbers $p_{\min}$ were distributed as $P(p_{\min}) \sim (p_c - p_{\min})^{(2-\tau)D\nu-1}$ close to p_c. Integrating over burst-size distributions in the range 0–p_c with the proper weight and cutoff he obtains $\tau_f^{\text{all}} = 2$.

The sequence of invaded random numbers also contains all the information we need for calculating the burst sizes, given the finite parameter κ and the finite growth zone length at each stage of the invasion. If a burst starts at a site with random number $p_{\min}$, the size of the following burst is found by drawing a straight line with a slope $1/(\kappa n_f)$ downwards until it hits the curve after s invaded sites, as indicated in Fig. 11. Since n_f fluctuates around some mean value, the downwards slopes will fluctuate too. In the limit $\kappa L^{D_f} \to \infty$, the lines are horizontal, so that if a site with random number larger than p_c is invaded, the following valley will sometimes "contain" the rest of the statistics.

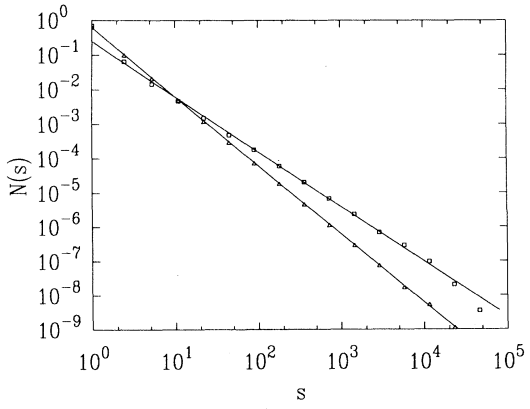

FIG. 12. Forward burst-size distribution for IP without trapping. Bursts start in narrow strip around p_c. System size $L_1 = 300$, average over 50 samples. Line of best fit has slope $\tau' = 1.60$. The lower curve is the distribution of hierarchical bursts, negative slope of line is $\tau_f^{\text{all}} = 2.0$.

VI. COMPARISON BETWEEN EXPERIMENTS AND SIMULATIONS

In this section we present results from the analysis of the experimental pressure curve in Fig. 3, namely, the burst or pressure jump distribution and the distribution of "composite bursts" or valleys in the pressure curve. The results are compared with simulations, where the simulation parameters have been estimated from the experiment.

We are at present uncertain whether our experimental front is best described by IP with the hull [20] or the external perimeter [19] as the growth zone model. The choice depends on the connectivity of the fluid phases, which in turn depends on how well the fluids wet the walls, the bead packing, and other effects. Reference [24] found a front corresponding to the external perimeter in simulations of drainage that included the detailed meniscus movements. Measurements of the fractal dimensions of experimentally invaded structures [36] are too uncertain to differentiate between the two trapping rules. It is also possible that experimental perimeters are a mixture of the two. In this section results from bond IP with external perimeter growth zone are compared with experiments.

We want to estimate the simulation parameters κ and L from the experiment. The number of pores along the baseline in the experiment is about $L = 100$, so that in the beginning of the experiment the front length is $n_f = 100$. The experimental change in capillary pressure per unit time $dp_{\text{expt}}/dt \simeq 0.06$ (mm H_2O)/s is estimated from the slope of the pressure curve (Fig. 3) in the buildup phase, where the water pressure decreases slowly. The extraction rate implies that the change of water volume along the front per time unit during buildup is $dV/dt = 0.048$ pores per second. This gives $\kappa_{\text{expt}} \simeq 0.008$ pores per mm H_2O for the experiment. The relevant property of the system is, however, not κ, but the average total capacity of the front to receive a water volume at the stage when a burst starts. This capacity depends also on the pressures where bursts start. In the simulations, capillary pressures where bursts start are found in the range 0–0.55 for systems of the same size as the experiment ($L = 100$), while in the experiments they are approximately within a range of 0–16 mm H_2O. The capillary pressure threshold distribution of the porous medium is unknown. *Assuming* a uniform distribution of capillary pressure thresholds in the porous medium gives the following linear relation between the experimentally measured pressures p_{expt} and the corresponding simulated pressures p_{cap}: $p_{\text{cap}} = 0.034[p_{\text{expt}}\ (\text{mm } H_2O)]$. Using this transformation, the estimate for κ becomes $\kappa \simeq 0.2$. Figure 13 shows the distributions of pressures where bursts start, p_{start}, for both experiments and simulations with

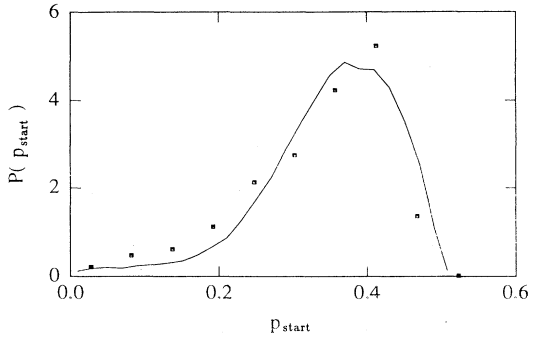

FIG. 13. Distribution of pressures where bursts start for the experiment (solid squares) and for simulations with $L_1 = 100$, $\kappa = 0.2$, 3500 invaded sites, averaged over 50 runs (solid line).

parameters estimated from the experiment. Since there is a good correspondence, we conclude that the capillary pressure threshold distribution in the porous medium is well described by a uniform distribution in the range of pressures where bursts start and therefore the range that governs the dynamics.

Figure 14 shows the exponentially decreasing cumulative pressure jump distributions for three different experiments together with matched simulations and a fitted exponentially decreasing curve. Pressures $P = \Pi/\langle\Pi\rangle$ are divided by $\langle\Pi\rangle$ which is the mean value of the pressure jumps Π above the experimental resolution of 0.1 mm water. Simulations are stopped after 750 bursts, which is the typical total number of bursts in an experiment.

Valleys in the pressure curve

The experimentally measured pressure jump size distributions are exponentially decreasing. With parameters corresponding to the experiment, also the simulated distributions are exponential, while for large values of the parameters L and κ, we obtain power-law distributions. We present a method that enables us to obtain latent power laws from the experimental pressure curves, even if the pressure jumps themselves are exponentially distributed. The method is inspired by that used for recognition of connected invaded regions from the sequence of random numbers in Sec. V D. However, in the case of the sequence of random numbers, the connected burst size is equal to the horizontal distance between crossings with a horizontal line. In the case of the pressure curve, connected composite bursts are proportional to the sum of the vertical jumps between horizontal crossings.

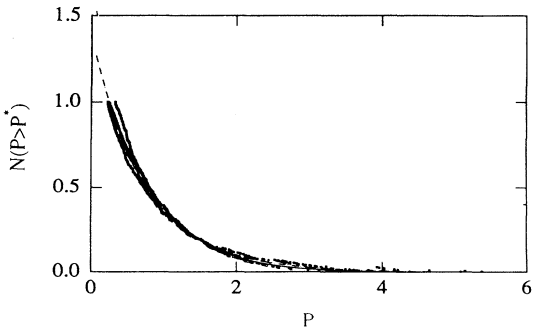

FIG. 14. Cumulative pressure jump distribution obtained from experiments and simulations with $\kappa = 0.2$, $L = 100$ (averaged over 100 runs). Dashed line: exponentially decreasing curve, $N(P > P^*) \propto e^{-1.31P^*}$. Solid line: simulations.

Consider a burst starting at a relatively high capillary pressure $p_{\mathrm{cap}}(t_1)$ (close to p_c), at time t_1 (see Fig. 5). In a system where the capillary pressure decreases quickly when one pore volume is invaded, the burst will not be able to proceed after invasion of only a few sites. The capillary pressure has to be increased again by extraction of water before new invasion can take place. If the capillary pressure starting the next burst is smaller than $p_{\mathrm{cap}}(t_1)$, both these bursts would have been included in a larger burst in a system where the pressure did not decrease significantly when pores were invaded. Only when the capillary pressure must be increased above $p_{\mathrm{cap}}(t_1)$ in order to start a burst, would the ideal system exhibit a new burst. A horizontal line drawn in the pressure curve (Fig. 3 or 5) beginning at $p_{\mathrm{cap}}(t_1)$ and ending where the capillary pressure curve is at the same level again at t_2 is defined to be a *valley* and it covers all burst that would have been included in one large burst starting at $p_{\mathrm{cap}}(t_1)$ in an ideal system. The time interval $(t_2 - t_1)$ is proportional (disregarding front length fluctuations that will average out) to the number of sites invaded at pressures smaller than $p_{\mathrm{cap}}(t_1)$ because when the pressure of the system is at the same level after a time $(t_2 - t_1)$, then the number of sites invaded in the mean time is roughly the volume injected into the system. Alternatively, all pressure jumps between t_1 and t_2 could have been added to get a composite burst which is proportional to the time difference $(t_2 - t_1)$.

We have chosen to find the size distribution of *all* valleys that start in a narrow strip of capillary pressures $(p_{\mathrm{min}} - p_{\mathrm{max}})$ only. This pressure range must be chosen in such a way that p_{min} is larger than p^* in order to extend

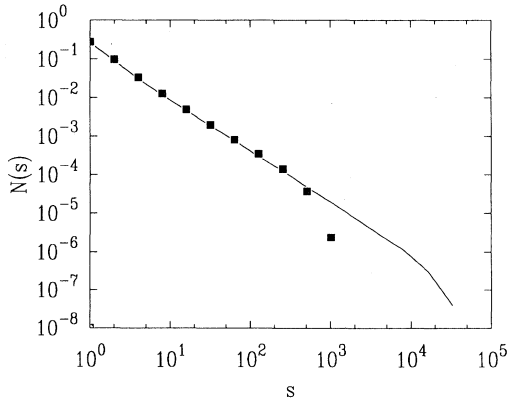

FIG. 15. Burst-size distribution (solid squares) and valley size distribution (full line), valleys starting between $p_{\mathrm{min}} = 0.49$ and $p_c = 0.50$ for simulated system with $\kappa = 10$, $L = 300$. The valley size distribution follows a power law in an extended regime.

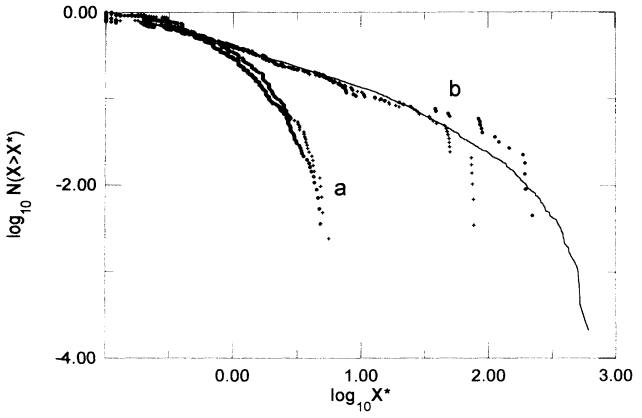

FIG. 16. (a): Exponential cumulative pressure jump distribution ($X = \Delta p_{\rm cap}$). (b) Cumulative valley size distribution for the experiments and the simulations. $X = \sum \Delta p_{\rm cap}$, where the sum is over one valley. Valleys start in a strip between $p_{\rm min} \simeq 14$ mm H_2O and 16 mm H_2O in the experiments. Computer simulation results for a corresponding system with $L_1 = 100$, $\kappa = 0.2$, 3500 invaded sites averaged over 50 runs (broken line).

the power-law regime of the valley distribution from that of the pressure jump distribution. In general the power-law range is extended further the closer to p_c the strip is chosen. Figure 15 demonstrates for a simulation how the valley size distribution gives a more extended power-law regime than the burst sizes for a system with $L = 300$ and $\kappa = 10$. In Fig. 16 the cumulative valley size distribution obtained from experiments with a strip in the pressure range 14–16 mm H_2O is presented, together with simulations with a strip in the range 0.45–0.50. The measured cumulative valley size distribution is consistent with a power-law behavior with an exponent $\tau' - 1 = 0.45 \pm 0.10$, which cannot be differentiated from the simulation result. In the simulations we observed a crossover between the exponents τ' and $\tau_f^{\rm all} = 2.0$ (see Sec. V D) when the strip became broader, so that the measured experimental slope 1.45 is probably a little larger than the "real" τ'. This favors an external perimeter growth zone as the best model for the experimental front.

All information of the bursts and valleys is contained in the curve of the sequence of random numbers (Fig. 11). We demonstrated that burst sizes were obtained from decreasing lines, while the parallel of valleys would be obtained with horizontal lines. However, the capillary pressure thresholds of the invaded throats are not available from the pressure measurements. Nevertheless, it is possible to extract the data from the pressure curve, which contains much less information.

VII. SUMMARY

Experiments in a quite small two-dimensional porous medium show that if water is extracted at a slow constant rate, air displaces the water in bursts. The distribution of burst sizes, assumed to be proportional to the jump heights of the pressure curve, was found to be exponentially decreasing. A modification of the well known IP model [4] included volumes assigned to the pores (sites) and an invader defined to be injected at a constant rate. The pressure was defined to be linearly dependent on the difference between the amount of "air" that was injected into the model and the number of sites invaded by "air." Parameters estimated from the experimental pressure curve gave results in good agreement with the experiment. Simulations of systems that had a larger capacity to receive a water volume when bursts started, exhibited a power-law distribution of burst sizes. The power-law exponents confirmed the connection to percolation exponents presented by Refs. [19,20]. By constructing a very large experiment, one would probably obtain the same power-law distribution for experimental bursts. Analysis of the experimental pressure curve, disregarding the splitting up of potentially large bursts due to the finite capacitive volume, indeed supports this hypothesis.

The burst-size distribution in simulations was earlier studied in Refs. [19,20] by modeling a steadily increasing pressure, and observing the bursts invaded when the pressure increased slightly. This procedure would have been very difficult to achieve in an experiment: The pressure would have to be instantaneously controlled, and the geometric burst sizes would have to be extracted from photographs. The present analysis gives the same information from the pressure fluctuations.

Reference [37] argues that the expression for the exponent τ' governing the burst-size distribution [Eq. (5)] is also valid for dimensions higher than the upper critical dimension $d \geq 6$. They expect the relation to hold also in three dimensions, but this needs to be tested.

ACKNOWLEDGMENTS

We thank E. Hinrichsen, T. Jøssang, S. Roux, A. Aharony, A. Hansen, P. Meakin, K. Christensen, V. Frette, U. Oxaal, and A. Birovljev for useful discussions. The authors gratefully acknowledge support from NFR, The Research Council of Norway.

[1] R. Lenormand and C. Zarcone, Phys. Rev. Lett. **54**, 2226 (1985).
[2] B. B. Mandelbrot, *The Fractal Geometry of Nature* (Freeman, New York, 1982).
[3] J. Feder, *Fractals* (Plenum, New York, 1988).
[4] D. Wilkinson and J. F. Willemsen, J. Phys. A **16**, 3365 (1983).
[5] P. G. de Gennes and E. Guyon, J. Mec. **17**, 403 (1978).
[6] R. Chandler, J. Koplik, K. Lerman, and D. Willemsen, J. Fluid. Mech. **119**, 249 (1982).
[7] K. J. Måløy, L. Furuberg, J. Feder, and T. Jøssang, Phys. Rev. Lett. **68**, 2161 (1992).

[8] W. B. Haines, J. Agric. Sci. **20**, 97 (1930).
[9] N. R. Morrow, Ind. Eng. Chem. **62**, 32 (1970).
[10] T. M. Shaw, Phys. Rev. Lett. **59**, 1671 (1987).
[11] M. Prat, Int. J. Multiphase Flow **19**, 691 (1993).
[12] A. H. Thompson, A. J. Katz, and R. A. Raschke, Phys. Rev. Lett. **58**, 29 (1987).
[13] A. J. Katz, A. H. Thompson, and R. A. Raschke, Phys. Rev. A **38**, 4901 (1988); J. N. Roux and D. Wilkinson *ibid.* **37**, 3921 (1988).
[14] P. Bak, C. Tang, and K. Wiesenfeld, Phys. Rev. Lett. **59**, 381 (1987); Phys. Rev. A **38**, 364 (1988).
[15] H. J. Feder and J. Feder, Phys. Rev. Lett. **66**, 2669 (1991).
[16] Z. Olami, H. J. Feder, and K. Christensen, Phys. Rev. Lett. **68**, 1244 (1992).
[17] A. Johansen, P. Dimon, C. Ellegaard, J. S. Larsen, and H. H. Rugh, Phys. Rev. E **48**, 4779 (1993).
[18] D. Stauffer and A. Aharony, *Introduction to Percolation Theory* (Taylor & Francis, London, 1992).
[19] N. Martys, M. O. Robbins, and M. Cieplak, Phys. Rev. B **44**, 12294 (1991).
[20] J. F. Gouyet and Y. Boughaleb, Phys. Rev. B **40**, 4760 (1989); J. F. Gouyet, Physica A **168**, 581 (1990).
[21] B. Sapoval, M. Rosso, and J. F. Gouyet, in *Fractals' Physical Origin and Properties*, edited by L. Pietronero (Plenum, New York, 1989).
[22] T. Grossman and A. Aharony, J. Phys. A **19**, L745 (1986); **20**, L1193 (1987).
[23] R. F. Voss, J. Phys. A **17**, L373 (1984); A. Bunde and J. F. Gouyet, *ibid.* **18**, L285 (1985); B. Sapoval, M. Rosso, and J. F. Gouyet, J. Phys. (Paris) Lett. **46**, L149 (1985); R. M. Ziff, Phys. Rev. Lett. **56**, 545 (1986); H. Saleur and B. Duplantier, *ibid.* **58**, 2325 (1987).
[24] M. Cieplak and M. O. Robbins, Phys. Rev. Lett. **60**, 2042 (1988); Phys. Rev. B **41**, 11 508 (1990); N. Martys, M. Cieplak, and M. O. Robbins, Phys. Rev. Lett. **66**, 1058 (1991).
[25] R. Lenormand and C. Zarcone, in *Proceedings of the Fifty-Ninth Annual Technological Conference and Exhibition of the Society of Petroleum Engineers* (Society of Petroleum Engineers, Richardson, TX, 1984); V. K. Horvath, F. Family, and T. Vicsek, Phys. Rev. Lett. **65**, 1388 (1990); J. Phys. A **24**, L25 (1991).
[26] K. J. Måløy (unpublished).
[27] P. Meakin, Physica A **173**, 305 (1991).
[28] A. Birovljev, L. Furuberg, J. Feder, T. Jøssang, K. J. Måløy, and A. Aharony, Phys. Rev. Lett. **67**, 584 (1991).
[29] S. Roux and E. Guyon, J. Phys. A **22**, 3693 (1989).
[30] Reference [29] suggested a different expression for τ', $\tau' = \tau - D_h/D$, where τ is the percolation cluster size exponent. In the case of external perimeter growth zone [7], this expression seems to correspond numerically with simulation results by chance. Gouyet [20] compared his *burst*-size distribution with the different *hierarchical forward burst*-size distribution of Ref. [29] in the case of hull growth zone and found by chance corresponding numerical exponents. In an attempt to derive the scaling of antired bonds in any dimension, the two different expressions for τ' were set equal in Ref. [38], and this led to erroneous results [37].
[31] S. Maslov, Phys. Rev. Lett. **74**, 562 (1995).
[32] M. F. Gyure and B. F. Edwards, Phys. Rev. Lett. **68**, 2692 (1992).
[33] J. F. Gouyet, Phys. Rev. B **47**, 5446 (1993).
[34] K. Sneppen, Phys. Rev. Lett. **69**, 3539 (1992).
[35] P. Bak and K. Sneppen, Phys. Rev. Lett. **71**, 4083 (1993).
[36] K. J. Måløy, F. Boger, J. Feder, and T. Jøssang, in *Time-Dependent Effects in Disordered Materials*, edited by R. Pynn and T. Riste (Plenum, New York, 1987).
[37] J. F. Gouyet, in *Soft Order in Physical Systems*, edited by R. Bruinsma and Y. Rabin (Plenum, New York, 1993).
[38] J. F. Gouyet, Physica A **191**, 301 (1992).